

Touch-free reactive flash sintering of dense strontium hexaferrite permanent magnet

Syed I. A. Jalali¹ | Alejandro F. Manchón-Gordón² | Ricardo Chacartegui³ | Pedro E. Sánchez-Jiménez^{2,4}  | Javier S. Blázquez⁵ | Antonio Perejón^{2,4}  | Rishi Raj¹  | Luis A. Pérez-Maqueda² 

¹Department of Mechanical Engineering, University of Colorado Boulder, Boulder, Colorado, USA

²Instituto de Ciencia de Materiales de Sevilla, ICMSE CSIC, Universidad de Sevilla, Sevilla, Spain

³Dpto. Ingeniería Energética, Universidad de Sevilla, Seville, Spain

⁴Departamento de Química Inorgánica, Facultad de Química, Universidad de Sevilla, Sevilla, Spain

⁵Dpto. Física de la Materia Condensada, ICMSE-CSIC, Universidad de Sevilla, Sevilla, Spain

Correspondence

Luis A. Pérez-Maqueda, Instituto de Ciencia de Materiales de Sevilla, ICMSE CSIC-Universidad de Sevilla, C. Américo Vespucio 49, Sevilla 41092, Spain.
 Email: maqueda@cica.es

Funding information

EU Next Generation; Spanish Ministry of Science and Innovation, Grant/Award Numbers: TED2021-131839B-C22, PDC2021-121552-C21, PID2022-140815OB-C22; Junta de Andalucía-Consejería de Transformación Económica, Industria, Conocimiento y Universidades, Grant/Award Number: ProyExcel_00360; Office of Naval Research, Grant/Award Number: N00014-18-1-2270; Fulbright Association, Grant/Award Number: PRX21/00434

Abstract

This work presents an extension of the touch-free flash sintering technique. In the proposed technique, chemical reaction and sintering occur in a single step, without the use of electrodes, in the presence of electric and magnetic fields. We show that a dense, single-phase strontium hexaferrite magnet can be produced from a mixture of commercial carbonate and oxide powders in a single step in a little more than a minute. This new technique implies significant reduction in energy and time consumption (primarily because of ultrafast processing) relative to conventional sintering.

KEY WORDS

permanent magnets, reactive flash sintering, strontium ferrite, touch-free flash sintering

1 | INTRODUCTION

The flash sintering (FS) technique, first proposed in 2010,¹ has drawn attention due to its environmental-friendly character, low sintering furnace temperatures, and short dwell times as compared to conventional sintering techniques.^{2–5} However, a real application of this technique is limited by the necessity of attaching electrodes that supply current to the workpiece. Since densification

is related to the current density,⁶ free form sintering would require a system of electrodes that maintain spatially uniform current in the workpiece. Recently, it has been shown that multiple electrodes can be used to sinter objects of an arbitrary shape.⁷ Very recently, it has been shown that flash can be induced without the use of electrodes, called touch-free FS,⁸ by the superposition of magnetic fields to the electrical field. Free form objects made from three yttria-stabilized zirconia (YSZ) were

This is an open access article under the terms of the Creative Commons Attribution License, which permits use, distribution and reproduction in any medium, provided the original work is properly cited.

© 2023 The Authors. *Journal of the American Ceramic Society* published by Wiley Periodicals LLC on behalf of American Ceramic Society.

sintered in this way. In a different approach, Saunders et al.⁹ used arc plasma electrodes for creating a conductive media for the current to pass to the pellet, achieving contactless FS. This method was used for sintering B_4C and $SiC:B_4C$ materials. Moreover, Dong et al.¹⁰ used a dielectric barrier discharge atmospheric cold plasma to sinter zirconia samples replacing the metallic electrodes. Besides, Johnson et al.¹¹ used flames both for heating and as electrode to prepare ceramic coatings on metallic substrates. A similar approach using flames was used by Lerdpram et al.¹² for glaze repair of sanitaryware bodies without the need for a kiln. Separately, we have shown that chemical reaction and sintering in multicomponent ceramics can occur in a single step by flashing mixtures of powders of constituent oxides: so-called reactive flash sintering (RFS).¹³ Since then, this technique has been applied to process ferrites,^{14,15} ferroelectrics,^{16,17} high-entropy oxides,^{18–21} and Li-ion ceramic electrolytes.^{22,23}

Here, we explore the application of the touch-free FS technique to RFS (TF-RFS), that is, preparation of multicomponent oxides by flash without the use of electrodes. We demonstrate this result to fabricate single-phase $SrFe_{12}O_{19}$ magnet from Fe_2O_3 and $SrCO_3$ powders. Strontium ferrite is considered a promising substitute for rare earth-based permanent magnets; it has high coercivity and good resistance to corrosion.²⁴

2 | EXPERIMENTAL

$SrFe_{12}O_{19}$ compound was synthesized from commercially available Fe_2O_3 and $SrCO_3$ powders (Sigma-Aldrich, ≥99% and ≥98% purity, and ≤5 and ~1 μm particle size, respectively). The precursor powders were dried in a warming oven to remove any moisture and mixed for 20 min in an Emax (Retsch) ball mill. Hardened steel balls and vials were employed as milling media. Powder mixtures were compressed into small pellets in a die at a pressure of 35 MPa. The dimensions of the green cylindrical pellet were ~6 mm in diameter and 2 mm in thickness. The pellets were placed within the reactor, and then flashed to full density by the application of magnetic field. The reactor consisted of a pre-sintered dog-bone specimen made from 8 mol% yttria-doped zirconia powder (Tosoh Corp.). The system configuration is shown in Figure 1a. The green sample pellet, that is, the workpiece, was held about 2 mm above the dog-bone using Kanthal wires that were electrically insulated from the electrical lines of the dog bones and the induction coil. The induction coil consisted of Kanthal wire with a diameter of 1.8 mm wrapped into 30 turns over a linear distance of 150 mm. The reactor and coil assembly were placed on a

linear motion assembly to be fed into the hot zone of a furnace heated up to 900°C at a rate of 10–25°C/min.

The electrical circuitry of the touch-free sintering apparatus used here consisted of two power supplies, one, a DC power supply to instigate flash in the dog-bone, and the other, the AC line voltage at 60 Hz, attenuated through a variac transformer, to power the induction coil. The flash in the zirconia dog-bones was initiated by applying a DC field of 100 V/cm while holding the furnace at 900°C. Flash is signaled by a sudden rise in conductivity. The maximum current flowing through the dog-bone was limited to a current density of 200 mA/mm². The current in the induction coil was increased from 0 to 50 A (AC) by turning the knob of the variac transformer. This process takes about 2–3 s.

The $SrFe_{12}O_{19}$ phase was characterized by X-ray diffraction using a Rigaku MiniFlex diffractometer (Cu-K α radiation) at room temperature. Le Bail fitting was performed using Topas Software. Scanning electron microscopy (SEM) images were obtained using a Hitachi S4800 SEM-FEG microscope operated at 10 kV. Magnetic hysteresis loops were obtained at room temperature using a maximum applied magnetic field of ±1.5 T in a vibrating sample magnetometer (Lakeshore 7407). The samples were rotated in the magnetic field to attain hysteresis loops at different conditions.

3 | RESULTS AND DISCUSSION

3.1 | Electrical activation parameters

The stages of the TF-RFS experiment are shown in Figure 1b–e. The evolution of electrical parameters (electric field and current density) are given as a function of time. The clock begins once the furnace reaches 900°C (time zero at point A). A field of 100 V/cm was applied to the zirconia dog-bone specimens with the DC power supply (point B). The sample conductivity rises nonlinearly, signaling the onset of flash, until the set current density limit of 200 mA/mm² is reached²⁵ (in about 30 s). At this point the power supply is switched from voltage control to current control. After holding the constant current density for 70 s, the current in the magnetic coil was instantaneously increased to 50 A (point C), which corresponds to an estimated magnetic field of ~0.125 T.⁸ At this point, magnetic field helps to concentrate plasma around the sample with the mixture of reactants,⁸ which, at this transition (point D), luminesces (as seen in the optical image). This is characteristic of a flash event. Note that the electric field required to maintain a constant value of the current density in the dog-bone specimen decreases.

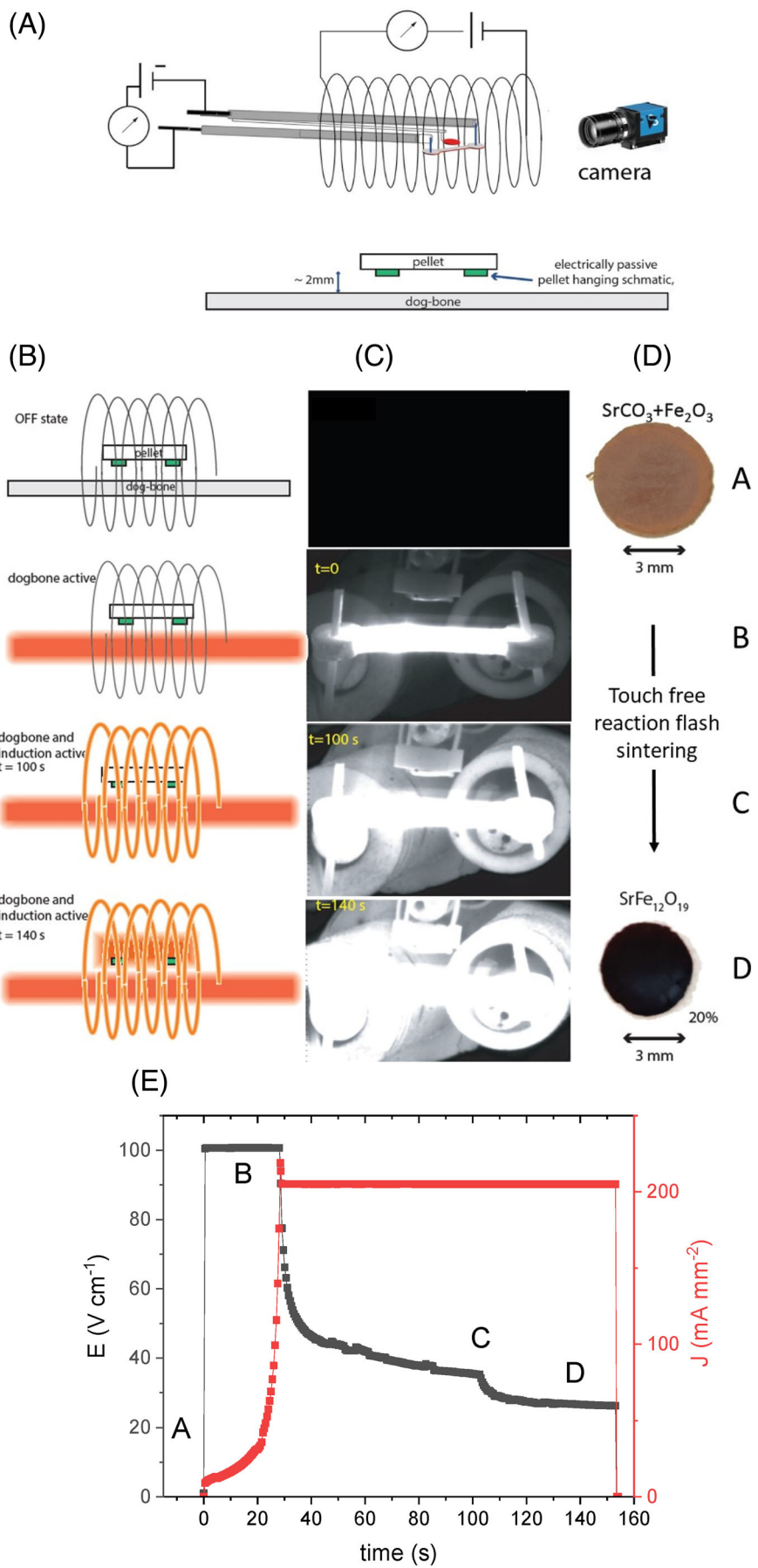


FIGURE 1 Touch-free sintering experiment using a DC power supply for the dog-bone and line AC (60 Hz) for induction. Schematic representation of (A) the touch-free setup and (B) the different stages of the experiment. (C) In operando images showing the onset of flash in the workpiece. (d) The pellet before and after the experiment. (E) The application of voltage to the dog-bones (A), switch to current control (B), application of magnetic field (C), and experiment ends at (D).

The sample is held in this stage for 55 s, and then, the system is switched off.

Note that the original, red color of the pellet (the work-piece), made from a mixture of Fe_2O_3 and SrCO_3 powders, transforms into a shrunken and sintered black pellet due to RFS. The linear shrinkage in the diameter of the pellet is about 20%, indicating nearly full densification. Thus, reaction into a single phase and densification occurred in a single step.

3.2 | Structural, microstructural, and magnetic characterization

The influence of the induction current on phase evolution was determined. In these experiments, the field and current density in the dog-bones were kept constant: DC field of 100 V/cm, furnace temperature of 900°C, and the current density limit of 200 mA/mm². In one case, an induction current of 20 A was employed, while in the second case, the current was increased to 50 A. Figure 2a shows the X-ray diffraction (XRD) patterns from these two cases. The presence of unreacted $\alpha\text{-Fe}_2\text{O}_3$ phase ($\bar{R}3c$ space group) in the sample prepared by applying 20 A in the induction coil indicates that for this intensity value, the induced magnetic field is insufficient for transferring the energy to form the $\text{SrFe}_{12}\text{O}_{19}$ phase. Interestingly, in a study on TF-RFS, it was observed that the higher the induction current was, the higher the density of the sample.⁸ Here, it is concluded that there is also a minimum value of induction current to induce the solid-state reaction in the touch-free experiment. When the current was increased to 50 A, no traces of the $\alpha\text{-Fe}_2\text{O}_3$ phase were detected and all reactants were converted, yielding phase-pure $\text{SrFe}_{12}\text{O}_{19}$ ($P6_3/mmc$ space group).

Le Bail fit to the XRD pattern of the monophasic sample is shown in Figure 2b. The “goodness” value of 1.2 illustrates the good quality of the fitting. The obtained lattice parameters were $a = 5.8796(2)$ Å and $c = 23.0674(3)$ Å, which are similar to those obtained for pure $\text{SrFe}_{12}\text{O}_{19}$ compound.²⁶

The microstructure of the cross-section fracture of the TF-RFSed pellet at an induction current of 50 A with a 1 min dwell time is shown in Figure 3a. The microstructure is a fairly homogeneous. Thus, the grain size distribution determined by averaging over 230 particles shows a mean value of $d \sim 0.8 \pm 0.1 \mu\text{m}$ with a narrow distribution. The microstructure represents a well-sintered, dense material, in agreement with the linear shrinkage in the pellet during FS. The relative density of the sintered sample was measured by the Archimedes' method using distilled water as the immersion liquid, obtaining a value of ~96% of the theoretical density (5.1 g/cm³ was employed as the theoretical density of $\text{SrFe}_{12}\text{O}_{19}$).²⁶

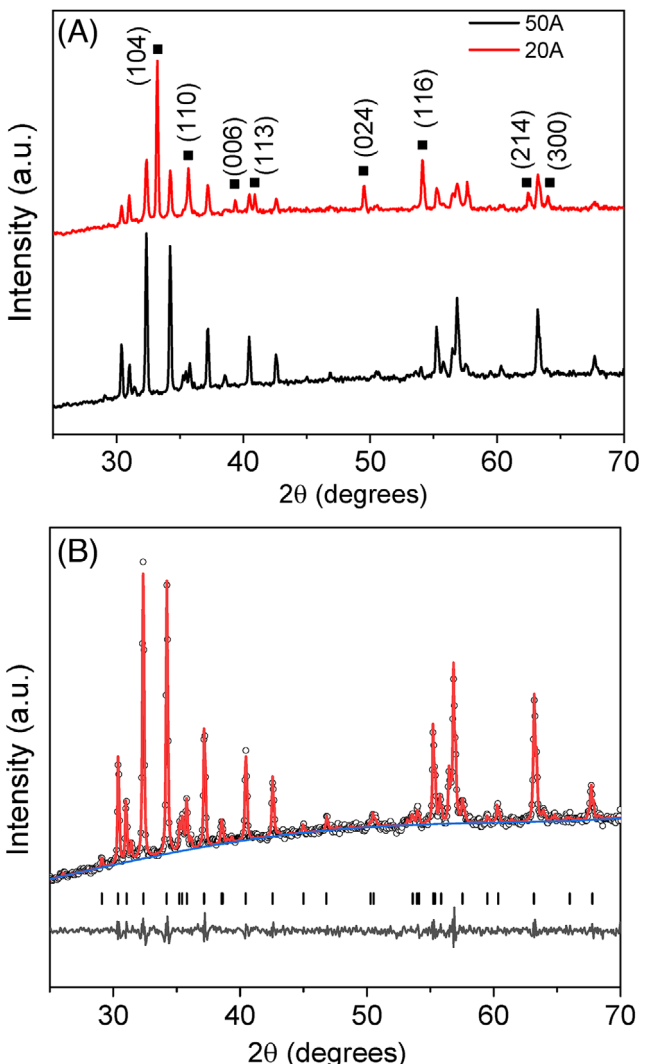


FIGURE 2 (A) X-ray diffraction patterns from pellets flash sintered with an induction current of 20 and 50 A. The indexed peaks correspond to the hematite ($\alpha\text{-Fe}_2\text{O}_3$) phase. (B) Le Bail fitting of the XRD pattern from the pellet obtained with an induction current of 50 A, that is, monophasic $\text{SrFe}_{12}\text{O}_{19}$ compound (JCPDS 33-1340).

The hysteresis loop $\sigma(H)$, where σ is the specific magnetization and H is the applied field, is shown in Figure 3b. The data were obtained at room temperature. Loops show high coercive field, H_C : a characteristic of hard magnets. The slope at high fields (which was limited by the equipment) gives information regarding saturation magnetization, σ_s . The reversibility confirms saturation at high fields.

In order to determine the existence of a preferred grain orientation, measurements were made by modifying the angle, θ , between the applied magnetic field, H , and sample's in-plane direction. A total of five hysteresis curves, carried out with a tilt angle increment of 15° from 0° to 90°, are included in Figure 3b (for simplicity, no demagnetizing factor has been considered). No significant differences can be observed in the loops; apparently, the application

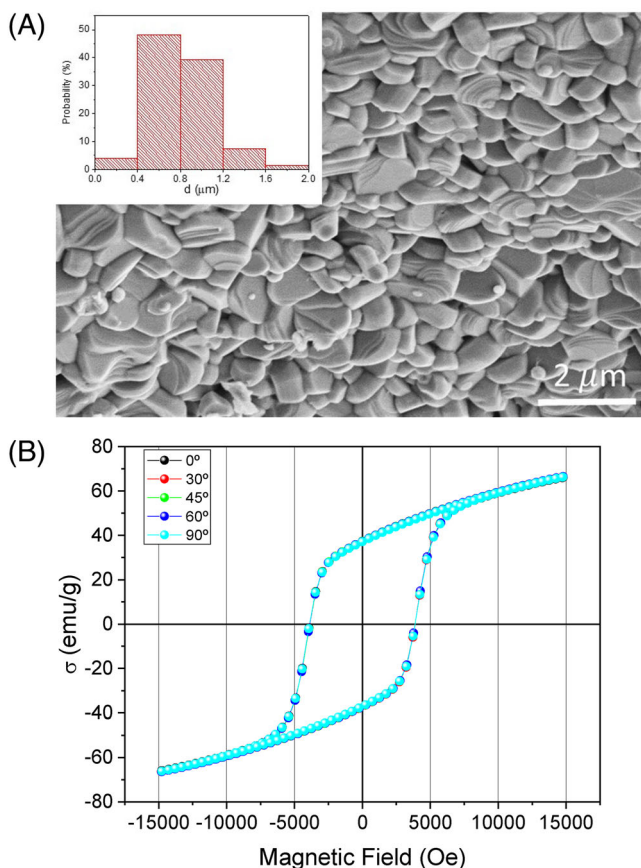


FIGURE 3 (a) Scanning electron microscopy (SEM) image of $\text{SrFe}_{12}\text{O}_{19}$ touch-free reactive flash sintered for 1 min at 900°C with an induction current of 50 A. Inset shows the histograms for the grain size. (b) Hysteresis loops at room temperature of the $\text{SrFe}_{12}\text{O}_{19}$ sample with the pellet tilted at the different angles relative to the external field.

of the magnetic induction current during TF-RFS did not produce preferred grain orientation.⁸

The saturation magnetization, σ_s , was derived from the Stoner-Wohlfarth model,²⁷ obtaining a value of 71.9 emu/g, a value higher than magnetization at 1.5 T, $\sigma_{1.5\text{T}} = 66.1$ emu/g. Furthermore, values of remnant magnetization, $\sigma_R = 37.2$ emu/g, and a coercive field, $H_C = 3.9$ kOe, were obtained. Note that the ratio σ_R/σ_s is close to 0.5, which is characteristic of samples with complete randomly oriented crystallites.²⁸ Similar values for σ_R/σ_s have been obtained in compounds prepared by conventional methods.²⁹

The energy product BH_{\max} is the figure of merit for hard magnets. It is associated with the energy stored in the magnetic field lines. This parameter, $BH_{\max} = 26 \text{ kJ/m}^3$, is comparable to the highest BH_{\max} value obtained for pre-aligned powders sintered by spark plasma sintering³⁰ and prepared by conventional RFS.¹⁵ In order to maximize the maximum energy product in permanent magnets, it is necessary to achieve a high degree of densification while

retaining significant H_C and σ_R . In the case of ferrites, sintering process often results in the loss of their hard magnetic properties, since the sintering temperatures required to achieve optimum densification, located between 1100°C and 1300°C , induce massive grain growth and significant loss in H_C .³¹ Therefore, the BH_{\max} obtained values after sintering are often far from the theoretical maximum value predicted for strontium ferrites (45 kJ/m^3).³² The obtained results in this work indicate the potential of the proposed technique to circumvent this problem due to the lowest temperatures required to obtain pure ferrite pellets, although there is room for improvement as the achieved value for BH_{\max} is still lower than the theoretical one for this material.

3.3 | Energy consumption analyses

The conventional preparation of $\text{SrFe}_{12}\text{O}_{19}$ magnets is an energetically intensive process. It usually requires two heating steps: first, the $\text{SrFe}_{12}\text{O}_{19}$ powder is prepared by heating a mixture of strontium carbonate and iron oxide at 1100°C for 2 h.³³ In the second step, the prepared powders are sintered at 1300°C for 4 h.³⁴ Figure 4 includes the values of energy and time consumption of a tubular furnace (GSL-1500X, MTI Corporation) for both conventional processes as measured with a power analyzer (PPA1500, Newtons4th Ltd.) directly connected to the furnace during the heating cycles. The resulting energy consumption value, as determined by integrating the power consumed by the furnace for the entire synthesis + sintering cycle, was $3 \times 10^8 \text{ J}$. In case of the TF-RFS process, the energy consumption is assigned (i) to heating the furnace up to 900°C and maintaining the furnace temperature during the entire process, and (ii) to the energy required for inducing the flash in the zirconia dog-bone and the energy consumed by the coil. In this case, the total energy consumed for preparing the material was $7 \times 10^6 \text{ J}$, that is, only about 2.5% of the energy consumed in conventional processing. The total time for the TF-RFS process, including furnace heating was approximately 15% of that required in the conventional method.

In actual practice, the furnace will be held at temperature, and the samples will be flash sintered, one after another in quick succession. Therefore, the process time will be much shorter than estimated just above; much lower energy consumption would be expected in large-scale production. In the same way, in a large-scale production of the conventional synthesis-sintering process, it should be expected the production of several tens to hundred samples in one run. Thus, a significant reduction in the energy consumption of the conventional procedures is expected due to the easily scalable technique. However,

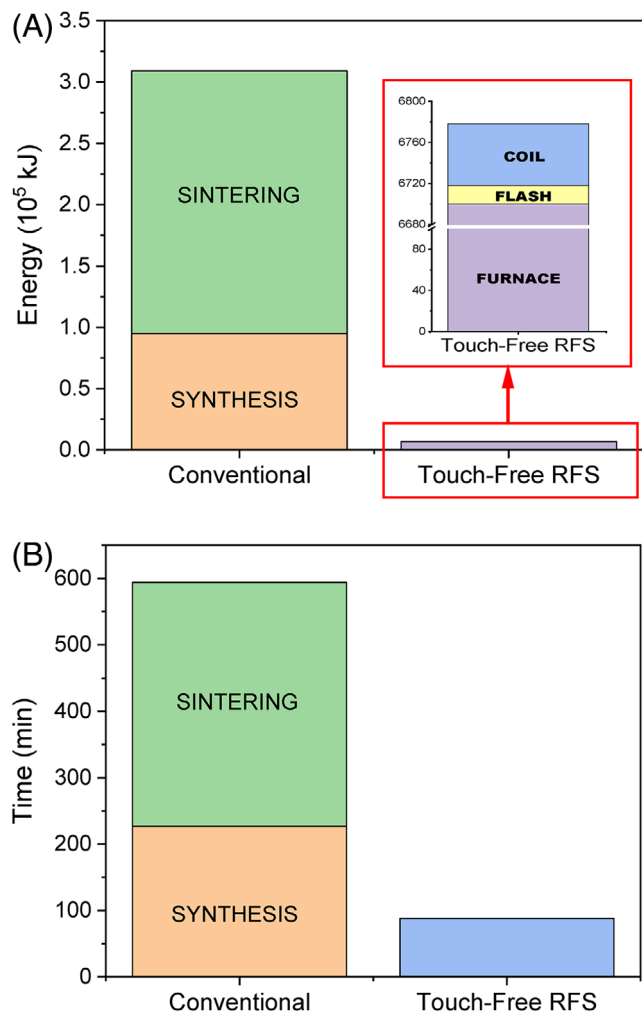


FIGURE 4 A comparison of (a) the energy and (b) the time needed for conventional and touch-free reactive flash sintering (TF-RFS) preparation of $\text{SrFe}_{12}\text{O}_{19}$. In the latter case, the energy needed for furnace heating, and for inducing the flash in the zirconia dog-bone and the energy consumed by the magnetic coil were considered.

there is no doubt that TF-RFS technique drastically reduces energy consumption when one-to-one sample is considered. Further studies will be required for precise energy consumption in real industrial applications.

4 | CONCLUSIONS

The viability of TF-RFS has been presented for the first time. In this process, a mixture of elemental oxides and carbonates is transformed into dense single-phase ferrite. The magnetic field enables “touch-free” processing without applying electrodes to the workpiece.

A mixture of strontium carbonate and iron oxide was used to produce a dense pure $\text{SrFe}_{12}\text{O}_{19}$ magnet within seconds and with a very narrow grain size distribution. The energy consumption in this process is

<15% of the conventional processing. The flash sintered sample shows magnetic properties comparable to those of samples prepared by conventional and spark plasma sintering procedures.

ACKNOWLEDGMENTS

This work was funded by EU Next Generation funds and/or the Spanish Ministry of Science and Innovation (grants TED2021-131839B-C22, PDC2021-121552-C21, and PID2022-140815OB-C22). Financial support received from Junta de Andalucía-Consejería de Transformación Económica, Industria, Conocimiento y Universidades (ProyExcel_00360) is also acknowledged. RR is grateful to the Office of Naval Research for supporting this research under the grant N00014-18-1-2270. RC acknowledges support from Fulbright Association (grant number PRX21/00434) for supporting his visit to Boulder.

ORCID

- Pedro E. Sánchez-Jiménez <https://orcid.org/0000-0001-6982-1411>
 Antonio Perejón <https://orcid.org/0000-0002-5525-2227>
 Rishi Raj <https://orcid.org/0000-0001-8556-9797>
 Luis A. Pérez-Maqueda <https://orcid.org/0000-0002-8267-3457>

REFERENCES

- Cologna M, Rashkova B, Raj R. Flash sintering of nanograin zirconia in <5 s at 850°C. *J Am Ceram Soc*. 2010;93(11):3556–9.
- Biesuz M, Sglavo VM. Flash sintering of ceramics. *J Eur Ceram Soc*. 2019;39(2):115–43.
- Raj R, Kulkarni A, Lebrun J-M, Jha S. Flash sintering: a new frontier in defect physics and materials science. *MRS Bull*. 2021;46(1):36–43.
- Gil-González E, Pérez-Maqueda LA, Sánchez-Jiménez PE, Perejón A. Flash sintering research perspective: a bibliometric analysis. *Materials*. 2022;15(2):416.
- Perez-Maqueda LA, Gil-Gonzalez E, Perejon A, Lebrun JM, Sanchez-Jimenez PE, Raj R. Flash sintering of highly insulating nanostructured phase-pure BiFeO_3 . *J Am Ceram Soc*. 2017;100(8):3365–9.
- Francis JSC, Raj R. Influence of the field and the current limit on flash sintering at isothermal furnace temperatures. *J Am Ceram Soc*. 2013;96(9):2754–8.
- Molina-Molina S, Gil-González E, Durán-Olivencia FJ, Valverde JM, Perejón A, Sánchez-Jiménez PE, et al. A novel multi-phase flash sintering (MPFS) technique for 3D complex-shaped ceramics. *Appl Mater Today*. 2022;26:101274.
- Jalali SIA, Raj R. Touch-free flash sintering with magnetic induction within a reactor activated by the usual flash method. *J Am Ceram Soc*. 2022;105(11):6517–22.
- Saunders T, Grasso S, Reece MJ. Ultrafast-contactless flash sintering using plasma electrodes. *Sci Rep*. 2016;6:27222.
- Dong J, Wang Z, Zhao X, Biesuz M, Saunders T, Zhang Z, et al. Contactless flash sintering based on cold plasma. *Scr Mater*. 2020;175:20–3.

11. Johnson SL, Venugopal G, Hunt AT. Flame-assisted flash sintering: a noncontact method to flash sinter coatings on conductive substrates. *J Am Ceram Soc.* 2018;101(2):536–41.
12. Lerdprrom W, Green C, Pearmain D. Contactless field enhanced sintering (cFES): a spot glaze repair technology (SGRT). *J Eur Ceram Soc.* 2022;42(5):2556–60.
13. Gil-González E, Perejón A, Sánchez-Jiménez PE, Sayagués MJ, Raj R, Pérez-Maqueda LA. Phase-pure BiFeO₃ produced by reaction flash-sintering of Bi₂O₃ and Fe₂O₃. *J Mater Chem A.* 2018;6(13):5356–66.
14. Manchón-Gordón AF, Sánchez-Jiménez PE, Blázquez JS, Perejón A, Pérez-Maqueda LA. Structural, vibrational, and magnetic characterization of orthoferrite LaFeO₃ ceramic prepared by reaction flash sintering. *Materials.* 2023;16(3):1019.
15. Manchón-Gordón AF, Sánchez-Jiménez PE, Blázquez JS, Perejón A, Pérez-Maqueda LA. Reactive flash sintering of SrFe₁₂O₁₉ ceramic permanent magnets. *J Alloys Compd.* 2022;922:166203.
16. Wu Y, Su X, An G, Hong W. Dense Na_{0.5}K_{0.5}NbO₃ ceramics produced by reactive flash sintering of NaNbO₃–KNbO₃ mixed powders. *Scr Mater.* 2020;174:49–52.
17. Taibi A, Chaguetmi S, Sánchez-Jiménez PE, Perejón A, García JE, Satha H, et al. Pure perovskite BiFeO₃–BaTiO₃ ceramics prepared by reaction flash sintering of Bi₂O₃–Fe₂O₃–BaTiO₃ mixed powders. *Ceram Int.* 2021;47(19):26947–54.
18. Mao H-R, Guo R-F, Cao Y, Jin S-B, Qiu X-M, Shen P. Ultrafast densification of high-entropy oxide (La_{0.2}Nd_{0.2}Sm_{0.2}Eu_{0.2}Gd_{0.2})₂Zr₂O₇ by reactive flash sintering. *J Eur Ceram Soc.* 2021;41(4):2855–60.
19. Yoon B, Avila V, Raj R, Jesus LM. Reactive flash sintering of the entropy-stabilized oxide Mg_{0.2}Ni_{0.2}Co_{0.2}Cu_{0.2}Zn_{0.2}O. *Scr Mater.* 2020;181:48–52.
20. Wang K, Ma B, Li T, Xie C, Sun Z, Liu D, et al. Fabrication of high-entropy perovskite oxide by reactive flash sintering. *Ceram Int.* 2020;46(11, Pt A):18358–61.
21. Li W, Chen L, Liu D, Liu J, An L. Ultra-low temperature reactive flash sintering synthesis of high-enthalpy and high-entropy Ca_{0.2}Co_{0.2}Ni_{0.2}Cu_{0.2}Zn_{0.2}O oxide ceramics. *Mater Lett.* 2021;304:130679.
22. Avila V, Yoon B, Ingraci Neto RR, Silva RS, Ghose S, Raj R, et al. Reactive flash sintering of the complex oxide Li_{0.5}La_{0.5}TiO₃ starting from an amorphous precursor powder. *Scr Mater.* 2020;176:78–82.
23. Avila V, Yoon B, Ghose S, Raj R, Jesus LM. Phase evolution during reactive flash sintering of Li_{6.25}Al_{0.25}La₃Zr₂O₁₂ starting from a chemically prepared powder. *J Eur Ceram Soc.* 2021;41(8):4552–7.
24. Lewis LH, Jiménez-Villacorta F. Perspectives on permanent magnetic materials for energy conversion and power generation. *Metall Mater Trans A.* 2013;44(1):2–20.
25. Naik KS, Sglavo VM, Raj R. Flash sintering as a nucleation phenomenon and a model thereof. *J Eur Ceram Soc.* 2014;34(15):4063–7.
26. Pullar RC. Hexagonal ferrites: a review of the synthesis, properties and applications of hexaferrite ceramics. *Prog Mater Sci.* 2012;57(7):1191–334.
27. Tannous C, Gieraltowski J. The Stoner–Wohlfarth model of ferromagnetism. *Eur J Phys.* 2008;29(3):475.
28. Stoner EC, Wohlfarth E. A mechanism of magnetic hysteresis in heterogeneous alloys. *Philos Trans R Soc Lond Ser A Math Phys Sci.* 1948;240(826):599–642.
29. Pérez-Juache T, Guerrero A, Cabal-Velarde J, Mirabal-García M, Palomares-Sánchez S, Matutes-Aquino J. Analysis of the structure and Mössbauer study of the neodymium substitution in the Sr-hexaferrite. *Phys B.* 2016;503:183–8.
30. Stingaci M, Eikeland AZ, Gjørup FH, Deledda S, Christensen M. Optimization of magnetic properties in fast consolidated SrFe₁₂O₁₉ nanocrystallites. *RSC Adv.* 2019;9(23):12968–76.
31. Dho J, Lee EK, Park JY, Hur NH. Effects of the grain boundary on the coercivity of barium ferrite BaFe₁₂O₁₉. *J Magn Magn Mater.* 2005;285(1):164–8.
32. Coey J. Hard magnetic materials: a perspective. *IEEE Trans Magn.* 2011;47(12):4671–81.
33. Faloh-Gandarilla JC, Díaz-Castañón S, Watts BE. Magnetization reversal and interactions in SrFe₁₂O₁₉. *Phys Status Solidi B.* 2017;254(4):1600393.
34. Guzmán-Mínguez JC, Vicente-Arche LM, Granados-Miralles C, Fernández JF, Quesada A. Improvement of the magnetic properties of SrFe₁₂O₁₉ ceramics by tailored sintering with SiO₂ addition. *J Alloys Compd.* 2021;860:157890.

How to cite this article: Jalali SIA, Manchón-Gordón AF, Chacartegui R, Sánchez-Jiménez PE, Blázquez JS, Perejón A, et al. Touch-free reactive flash sintering of dense strontium hexaferrite permanent magnet. *J Am Ceram Soc.* 2023;106:7202–7208.
<https://doi.org/10.1111/jace.19389>